

3 Modeling Amyloid Fibrillation

Amyloid fibrillation has been intensively studied because of its association with various neurological disorders. While extensive time-dependent fibrillation experimental data are available and appear similar, few mechanistic models have been developed to unify those results. The aim of this work was to interpret these experimental results via a rigorous mathematical model that incorporates the physical chemistry of nucleation and fibril growth dynamics. A three-stage mechanism consisting of protein misfolding, nucleation, and fibril elongation is proposed and supported by the features of homogeneous fibrillation responses. Estimated by nonlinear least squares algorithms, the rate constants for nucleation were about ten million times smaller than those for fibril growth. These results, coupled with the positive feedback characteristics of the elongation process, account for the typical sigmoidal behavior during fibrillation. In addition, experiments with different proteins, various initial concentrations, seeding versus non-seeding, and several agitation rates were analyzed with respect to fibrillation using our new model. The wide applicability of the model confirms that fibrillation kinetics may be fairly similar among amyloid proteins and for different environmental factors. Recommendations on further experiments and on the possible use of molecular simulations to determine the desired properties of potential fibrillation inhibitors are offered.

3.1 Introduction of amyloid fibrillation

Amyloid fibrillation is the process of native soluble proteins misfolding into insoluble fibrils comprising cross- β -sheets. More than 20 amyloidogenic diseases such as Alzheimer's disease, Parkinson's disease, and prion-associated encephalopathies have been found to share fibril formation as the a common symptom [42]. While the presence of amyloid plaques correlates with disease, whether fibrils themselves, misfolded oligomers, or other factors are the causal agents of diseases remains unclear [3, 4, 18]. Although the proteins associated with each disease do not share sequence homology, they exhibit similar insoluble filaments and fibrillation responses [15, 39]. This suggests that the underlying fibril formation mechanisms may be common [14].

The typical fibril formation process starts with a lag phase in which the amount of amyloid proteins turned into of fibrils is not significant enough to be detected. Afterwards, a drastic elongation phase follows and fibril concentration increases rapidly [32]. Eventually, the process reaches equilibrium when most soluble proteins are converted into fibrils. The length of lag times and fibril growth rates depend upon factors like the initial concentration and pH, both of which affect the degree of super-saturation in solution. The presence of seeded molecules and foreign surfaces can influence the kinetics of fibrillation, because of the ability to catalyze the reactions at these interfaces [43]. Other factors include the ionic strength of the solution and the intensity of agitation

[30]. Although experimental data covering these many different conditions have been reported in the literature, there is a noticeable lack of quantitative mechanistic models to provide insight into the process and directions for further research.

Because of the commonly observed sigmoidal-shaped fibrillation response reported in the literature [5, 30], fibrillation processes have been modeled as a number of reactions in series covering the assembly of oligomers, the formation of nuclei as well as the growth and the breakage of fibrils [4, 6, 24]. Moreover, the two-stage mechanism of yeast prion fibrillation, in which fibrils act as enzymes to trigger nucleated conformational conversion by Michaelis-Menten kinetics, provides another valuable perspective [36]. Empirical or semi-empirical exponential functions are popular choices to fit the data since they are computationally simple and match the observed data well [30, 34]. While suggestive, some of these models only depicted the sigmoidal trend without rigorous quantitative arguments; others have not provided details on how the nuclei form or explained the shortened lag-time resulting from seeding and an increase in the initial protein concentration.

The lag-time prior to fibril growth has been noted in numerous publications and resembles an incubation period [5, 30]. Explaining its existence is one of the key scientific challenges. The problem was approached by Shoghi-Jadid et al. [41] with introduction of the Heaviside function to force the separation of nucleation and fibrillation processes, while Uversky et al [44] used an empirical exponential model with adjustable parameters. We suggest that nucleation theory and growth models could be valuable in describing the fibrillation process. Furthermore, the drastic rate increase in the fibrillar growth phase after the lag phase indicates that cooperativity or positive feedback mechanisms are involved.

Another critical but missing piece of information is the relationship between the observable response and the degree of fibrillation. Even though histological dyes like thioflavin T (ThT) and Congo Red have been commonly used as indicators of the presence of amyloid fibrils, the relationship between fluorescence intensity and amount of amyloid fibril remain unclear [21, 22]. There are also physical property methods for measuring fibril formation like turbidity, absorbance and sedimentation [5, 40]. Here, we assumed linearity between ThT fluorescence and fibril concentrations based on Beer-Lambert law as a measure of fibril content, and use ultraviolet-visible (UV-vis) absorbance at 280 nm as a quantitative measure of dissolved total protein.

Insulin (51 aa; 6 kDa) was chosen as the model protein for the measurements in this study because it (i) is a well-studied fibril-forming protein and has recently been studied in our laboratory [19], (ii) has been crystallized in the native state at high resolution, (iii) is known to develop structurally similar cross- β -sheet plaques to those formed by other amyloids, and is deposited in arterial walls of type II diabetes patients [45], and (iv) is available in large quantities at reasonable price. Native insulin is well-folded and in stable hexamer state associated with Zn^{2+} molecule under physiological conditions. Yet it can be readily unfolded to form fibrils in solution by both increasing the temperature to 65°C and by reducing the pH to 1.6. Jiménez et al. proposed that the α -helical structure

(58%) of native insulin becomes unfolded to expose the β -sheet region (6%) which is the major component of the amyloid cross- β ribbon [13].

In the next section, we describe the proposed kinetic model for insulin fibrillation including the parameter estimation procedure. Since experimental protocols and responses of fibrillation are similar among amyloid proteins, the modeling approach presented here is also applicable to the fibrillation of other proteins. Afterwards, our model is compared with an empirical fitting function. A general description of the Experimental Materials and Methods follows. Then, in the Results and Discussion section, the new model is fitted to our insulin fibrillation data, to fibrillation of A β -40 and prion-like NM fragment of Sup-35 [5, 17], and to data conducted under various conditions (i.e. increasing initial insulin concentration, effect of seeding, stirring effects).

3.1.1 A kinetic model for insulin fibrillation

Three standard analytical steps were chosen to model insulin fibrillation: formulation of the appropriate kinetic reactions based on the polymerization and nucleation theories, conversions of the reaction set into a system of differential equations, and parameter estimation by nonlinear least square algorithms to optimize the fit between simulation results and the experimental measurements.

Initially four species of insulin were considered during fibrillation: original hexamer, monomer, cluster, and fibril [33, 40]. While the original hexamer is composed of six monomers stabilized by Zn^{2+} , an insulin monomer refers to two chains of polypeptides connected with disulfide bonds (the A- and B-chains comprising 21 and 30 amino acids, respectively). For systems other than insulin, different morphologies may be involved such as those for β_2 -microglobulin [9]. By incorporating the four insulin species into the reaction scheme, the proposed kinetic mechanism for this study consists of three distinct stages: decomposition of hexamers, nucleation process, and fibrillation stage as summarized in Figure 3-1 and Table 3-1. All the reactions listed are elementary reactions so the fluxes can be easily expressed as the products of reactant concentrations and the rate constant. Regarding notations, A_{hex} and A_i denote the concentration of original insulin hexamers and oligomers containing i monomers, respectively. All fibrils are abbreviated as F , regardless of their length. Even though physical reactions contributing to larger-size cluster formation and the entanglement between strands of fibrils have been reported [13, 25], the actual active chemical reaction sites are assumed to be restricted to the fibril ends [40]. Therefore, fibrils of different sizes can be considered as the same species.

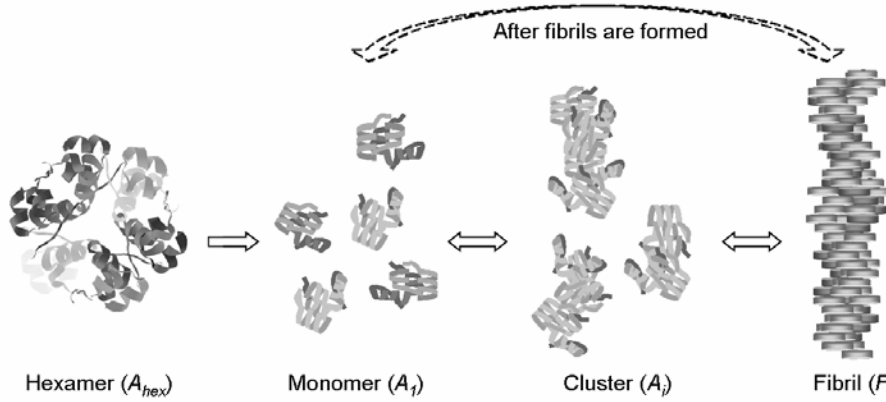


Figure 3-1 The key species in the proposed three stage reaction mechanism of insulin. The images of the hexamer and fibril were redrawn based on the literature [8, 13].

Key reaction species interact with one another and reactions proceed as summarized in Table 3-1. A nomenclature table that summarizes the meanings of symbols is attached at the end (Table 3-3). First, the zinc-stabilized hexamers are assumed to irreversibly misfold and dissociate into monomers containing cross β -sheets under stringent conditions like low pH and high temperature [31]. Since the dissociated form of insulin has been reported to readily misfold into reactive monomers [13], the misfolding step is assumed to occur very fast. In this case, the dissociation step is rate limiting with the rate constant k_d . Second, the mechanism of nucleation is based on the Becker-Döring nucleation model from the field of atmospheric science [38]. Accordingly the newly formed monomers react with one another as well as with different size oligomers so as to become larger clusters. The reactions between larger oligomers are negligible because their early concentrations and diffusivities are relatively low and small, respectively, as compared with the monomers. As oligomers grow, their chemical potentials drop, yet the surface tension to form new phases rises. Hence, there should exist a condition with minimum Gibbs free energy corresponding to the size of a cluster (or nuclei), $(n-1)$ -mer [38]. Any aggregates larger than the cluster would convert into fibrils. Once the fibrils are formed, their ends serve as nuclei and undergo self catalytic reactions to become longer fibrils with $k_{fb,i}$ and $k_{fb,-i}$ as the forward and reverse rate constants [10]. At this stage, reactions between fibrils and all sizes of oligomers need to be taken into account since the reactive nature of fibril ends greatly accelerates the process. Finally, the reactions of i -mer addition and detachment proceed until the clusters are depleted and reach equilibrium with fibrils.

After the kinetic schemes are established, the concentrations of various species are expressed as functions of time. The temporal change of these species can be derived from material balances and reaction kinetics. The first specie to be considered is the original insulin hexamer whose rate of change is expressed as the disappearance by dissociation (Eq. (1.1)).

$$\frac{dA_{hex}}{dt} = -J_d \quad (1.1)$$

The rate of monomer concentration change can be calculated by taking into account all the reactions involving monomers in Table 3-1. As a result, the time derivative of A_1 equals the generation rate from the hexamer dissociation reaction minus the consumption rate due to all nucleation reactions, and the first elongation reaction (Eq. (1.2)). The constants before J_d and $J_{nu,1}$ are the stoichiometric coefficients.

$$\frac{dA_1}{dt} = 6J_d - 2J_{nu,1} - \sum_{i=2}^{n-1} J_{nu,i} - J_{fb,1} \quad (1.2)$$

Then the concentration change of i -mer clusters is equal to its formation rate from the $(i-1)$ -th nucleation reaction minus the consumption rate due to the i -th nucleation reaction and the i -th elongation reaction (Eq. (1.3)).

$$\frac{dA_i}{dt} = J_{nu,(i-1)} - J_{nu,i} - J_{fb,i} \quad \text{for } i = 2, 3, \dots, n-1 \quad (1.3)$$

The addition of monomer to the largest possible cluster (A_{n-1}) results into fibril formation as the last reaction at the nucleation stage suggests. Hence, the time derivative of fibril concentration is equal to the fibril generation rate subtracted by its consumption rate, i.e., the net flux of last nucleation reaction (Eq. (1.4)). Note that the fibril elongation process actually does not affect fibril concentration since no additional fibrils are formed or consumed at that stage.

$$\frac{dF}{dt} = k_{nu,(n-1)}A_1A_{n-1} - k_{nu,-(n-1)}F \quad (1.4)$$

The initial concentration of insulin hexamers is equal to the amount of insulin added initially and is the main driving force for the downstream reactions (i.e., $A_{hex}=A_{hex0}$). The concentrations of the other species are assumed to be zero at the start (i.e., $A_i=0$, $F=0$). Eqs. (1.1)-(1.4) contain totally $n+1$ variables with equal number of corresponding differential equations and initial conditions. Thus, the system of differential equations is properly defined and ready to be solved once the values of all parameters are specified.

Even though the model contains quite a few parameters, some of them are physically related to one another; others can be found from the literature. Three assumptions were made to reduce the total number of parameters.

1. The value of n , the critical number of monomers needed to form a nucleus, has been reported as six [41], so initially we have set n equal to six. However, we also discuss the sensitivity of this parameter on the model fit in the section “*In vitro* fibrillation kinetics”. The dissociation rate constant of insulin k_d can be estimated from the insulin dissociation time of about one hour [11]. Assuming that one hour is approximately the time to reach 95% conversion of exponential decay, k_d is $\sim 3 \text{ h}^{-1}$.

2. Since agitation has been found to drastically shorten the delay time [43], the reaction rates of forward nucleation and fibrillation ($k_{nu,i}$ and $k_{fb,i}$) are assumed to be diffusion limited [40]. Apparent rate constants of diffusion controlled reactions take the form of Eq. (1.5) [7], in which \tilde{N} is Avogadro's number, d_{AF} is the mean free path of the complex molecule, and D_A+D_F is the sum of diffusivities of the reactants. The values of diffusivities are proportional to the inverse of the characteristic length R_{Ai} , following Stokes-Einstein equation as in Eq. (1.6) [2]. The volume of i -mer is equal to i times the volume of the monomer (V_1) and is also related to its own characteristic radius (R_{Ai}) through volumetric formula. Thus, the diffusivity is roughly proportional to the inverted cubic root of i , which equals the size of the cluster.

$$k_D = \tilde{N}4\pi(D_A + D_F)d_{AF} \quad (1.5)$$

$$D_{A_i} \propto \frac{1}{R_{A_i}} = \frac{1}{\sqrt[3]{\frac{3}{4\pi}iV_1}} \propto \frac{1}{\sqrt[3]{i}} \quad (1.6)$$

In Eqs. (1.5) & (1.6), nucleation and fibrillation forward rate constants regarding different sizes of oligomer can be approximated by Eq. (1.7) and Eq.(1.8). Because the sizes of oligomers are comparable and thus their diffusivities are similar, both diffusivities need to be taken into account in the nucleation process. On the other hand, in the case of fibrillation, since the sizes of fibrils are much larger than those of oligomers, D_F is negligible compared to D_{A_i} and therefore, the diffusivity of the oligomer is the dominant term.

$$k_{nu,i} = \frac{1}{2}k_{nu,1}\left(1 + \frac{1}{\sqrt[3]{i}}\right) \propto 4\pi(D_{A_i} + D_{A_1}) \quad (1.7)$$

$$k_{fb,i} \approx k_{fb,1}\frac{1}{\sqrt[3]{i}} \propto 4\pi D_{A_i} \quad (1.8)$$

3. The values of $k_{nu,i}$ and $k_{fb,i}$ are assumed to be independent of size i , and are abbreviated as k_{nu-} and k_{fb-} respectively. Serio et al. showed that sonicated seeding provided a larger amount of fibril ends as reactive sites and demonstrated higher reaction rate [40]. This suggested that under normal condition, the detachment of oligomers often occurs at the terminal rather than in the internal segment. Hence, for this study, the number of monomers within a chain or oligomer does not affect the reverse rate significantly.

3.1.2 Parameter estimation and model comparison

The predictions of Eqs.(1.1)-(1.4) were compared with the experimental data (i.e. values of the species concentrations) in order to estimate the rate constants. There were

four kinds of observable data considered: ThT fluorescence, UV-Vis absorbance at 600 nm (A_{600}), turbidity, and dissolved insulin concentrations (absorbance at 280 nm, A_{280}). The first three measures were assumed to be roughly proportional to the insulin fibril concentrations by Beer-Lambert law [22], and denoted as $Y = b \cdot F$. The last measure was simulated by counting total number of i -mers in the unit of monomer concentration, which could be expressed as $Y = \sum_i A_i \cdot i$. Nonlinear least square regression was adopted to minimize the sum of squared errors between experimental data and those predicted by the model; parameter estimation procedures were carried out in Matlab[®]. Detailed algorithms are given in the Supplemental Materials [37].

Table 3-1. The proposed three-stage model including reaction fluxes and rate constants

Description of Processes	Reaction Schemes	Reaction Fluxes
Hexamer Decomposition	$A_{hex} \xrightarrow{k_d} 6A_1$	$J_d = k_d A_{hex}$
Nucleation Stage	$A_1 + A_1 \xrightleftharpoons[k_{nu,-1}]{k_{nu,1}} A_2$ $A_1 + A_2 \xrightleftharpoons[k_{nu,-2}]{k_{nu,2}} A_3 \dots\dots$ $A_1 + A_{n-2} \xrightleftharpoons[k_{nu,-(n-2)}]{k_{nu,(n-2)}} A_{n-1}$ $A_1 + A_{n-1} \xrightleftharpoons[k_{nu,-(n-1)}]{k_{nu,(n-1)}} F$	$J_{nu,i} = k_{nu,i} A_1 A_i - k_{nu,-i} A_{i+1}$
Elongation Stage	$F + A_1 \xrightleftharpoons[k_{fb,-1}]{k_{fb,1}} F$ $F + A_2 \xrightleftharpoons[k_{fb,-2}]{k_{fb,2}} F \dots\dots$ $F + A_{n-1} \xrightleftharpoons[k_{fb,-(n-1)}]{k_{fb,(n-1)}} F$	$J_{fb,i} = k_{fb,i} A_i F - k_{fb,-i} F$

In the past, an empirical function like Eq. has been used in the literature to fit the fluorescent ThT data with time data [30, 44]. Independent of the amyloid protein type, Eq. (1.9) fits the fibrillation data reasonable well. This again suggests that the fibril formation process is similar for these different proteins. It is a specialized form of the logistic function which has been frequently used in the field of population biology [16]. The parameters from this model include the apparent rate constant for the growth of fibril (k_{app}), and the lag time which are equal to $1/\tau$ and $t_0-2\tau$, respectively.

$$Y = y_i + \frac{y_f}{1 + e^{-(t-t_0)/\tau}} \quad (1.9)$$

In the Supplemental Materials, it is shown how to relate the parameters in this empirical model to the kinetic rate constants in Eqs. (1.1)-(1.4) under simplifying assumptions. That is, when the critical size of a nucleus (n) is equal to 2, there is an analytical solution for the only two species, A_1 and F . By mass balance, $A_1 = A_0 - F \cdot N$ (where A_0 is initial concentration and N is the average fibril size). The time derivative for the fibril concentration can be reduced to a quadratic differential equation (Eq. (1.10)). The two roots of the equation, r_1 and r_2 , are obtained from the quadratic formula and correspond to the steady state fibril concentrations. Eq. (1.11) is the solution of Eq. (1.10) by integration. It expresses the temporal evolution of the fibril concentration, and has the equivalent functional form of Eq. (1.9). The observable delay lag and growth rates can be related to the kinetic constants by Eq. (1.12).

$$\frac{dF}{dt} = k_{nu,1}A_1^2 + k_{fb,1}FA_1 - k_{fb-}F \propto -(F - r_1)(F - r_2) \quad (1.10)$$

$$F = r_1 + \frac{r_2 - r_1}{1 + e^{-(t-t_0)/\tau}} \quad (1.11)$$

$$\frac{1}{\tau} = (Nk_{fb,1} - N^2k_{nu,1})(r_2 - r_1) \quad \text{and} \quad t_0 = \tau \ln(-r_2 / r_1) \quad (1.12)$$

3.2 Experimental Procedures

All chemicals were obtained from Sigma Chemical Co. (St. Louis, MO). Recombinant human insulin was generously donated by Novo Nordisk A/B, Denmark. All insulin solutions used for the *in vitro* fibril formation experiments were freshly prepared prior to each experiment in 0.025 M HCl, 0.1 M NaCl and adjusted to pH 1.6. Each sample for the kinetic experiments contained 1 ml of 2 mg/ml insulin in glass vials and was incubated at 65°C. At appropriate time intervals, the sample was removed from the incubator for analysis.

UV-Vis absorbance assay: *In vitro* insulin fibril formation has been shown to result in the formation of insoluble aggregates which are β -sheet rich structures [30]. The UV-

visible absorbance assay at 600 nm wavelength (A_{600}) has been extensively used to quantify insoluble aggregates like inclusion bodies and cell debris from cell culture and is also used frequently molecular biology studies. Here, we quantify the amount of insoluble protein (fibrils) and soluble protein by measuring the absorbance of the solutions at 600 nm and 280 nm, respectively. The absorbance was measured on a Hitachi U 2000 Double-Beam UV/VIS spectrophotometer (Hitachi Instruments Inc., Danbury, CT). Spin-x centrifuge tube filters (Corning Inc., NY) of 2 ml total volume with 0.22 μm pore size cellulose acetate membranes were used for separating the fibrils from the soluble protein. Centrifugation was conducted at 10,000g for 10 min to separate the fibrils from the supernatant. Then, the protein concentration in the supernatant was measured at 280 nm using a calibration curve.

3.3 Results and discussion

The model is first fitted to the data from our laboratory for the fibrillation of human recombinant insulin. We then tested the model with the experimental dataset from the literature, including fibrillation data of other proteins, at different initial concentrations, with and without seeding, and at different stirring rates. In addition, the kinetic rate

3.3.1 *In vitro* fibrillation kinetics

Two experimental assays were followed during the *in vitro* insulin fibrillation process. The UV-visible absorbance assay at 600 nm wavelength (A_{600}) was used to follow the formation of fibrils and A_{280} was used to track total protein after removing the fibrils with microfiltration. As seen in Figure 3-2A, the two sets of data closely followed each other with a sigmoidal and inverse sigmoidal curve. This result demonstrates that mass from the dissolved protein was used to form the fibrils and that the mass balance closed fairly well. To test the validity of the first assumption regarding n , the critical size of nucleus, the data in Figure 3-2A was fit with different values of n (results not shown). The R^2 value was the highest for n equal to six and dropped below 0.9 for n smaller than four or larger than nine. While nucleus sizes may take different values, statistically six was the least-squares estimator that minimized the sum of squared errors. Thus, the assumption of $n \sim 6$ is reasonable for this study. Further experiments that measure fibril size distribution with time are clearly needed.

Since two independent measurements, A_{600} , and A_{280} , were used to follow the gain in fibrils and loss in protein with time, respectively, the model was first fit to each separate set of data and then to both sets of data simultaneously to obtain the values of the rate constants listed in Table 3-1 together with the goodness-of-fit estimates. First, the values of $k_{nu,1}$ are about 8 order of magnitude smaller than those of $k_{fb,1}$, which confirms the widely held view that the nucleation rate was rate limiting and that fibrillation was extremely fast. For fits of both sets simultaneously (combined), the rate constants were $k_{nu,1} = 3.74 \times 10^{-2} \text{ (h}^{-1}\text{mM}^{-1}\text{)}$, $k_{nu-} = 1.01 \times 10^{-3} \text{ (h}^{-1}\text{)}$, $k_{fb,1} = 2.75 \times 10^6 \text{ (h}^{-1}\text{mM}^{-1}\text{)}$, and $k_{fb-} = 1.84 \times 10^3 \text{ (h}^{-1}\text{)}$. This set of rate constants was then chosen for the sensitivity analysis reported in the Supplemental Materials to evaluate the impact of each

parameter. Since several folds of change in k_{nu-} barely altered the fibrillation profile, k_{nu-} was not further considered for the parameter optimization (Supplemental Material Figure S1).

Thermodynamically, the rate constants are related to the Gibbs free energy of transition from the monomer to the nuclei, $(n-1)$ -mer. By summing up all the reactions except the last one in the nucleation process in Table 3-1, we obtain Eq. (1.13) below. The standard Gibbs free energy can be calculated from equilibrium constants with Eq. (1.14) [38], where ΔG° denotes the free energy difference between monomers and $(n-1)$ -mer clusters. The higher the ratio of the forward to the reverse rate constant, the more likely will the monomers convert to nuclei. Our calculated value of ΔG° is 42.6 ± 12.2 kJ/mol, which is of the same order of magnitude as that reported for amyloid fibers, 33.4 kJ/mol [27]. Further, since the values of $k_{nu,i}$ are larger than k_{nu-} , the free energy should be negative and the nucleation process is spontaneous.



$$\Delta G^\circ = -RT \ln K_c = -RT \ln \prod_{i=1}^{n-1} \frac{k_{nu,i}}{k_{nu-}} \quad (1.14)$$

The model is also able to track various insulin species such as initial hexamers, monomers, dimers, other oligomers and fibrils. It can be seen from Figure 3-2B&C that (i) all the initial zinc stabilized hexamer had disappeared by ~ 2 h, (ii) monomer reached a maximum at ~ 1 h and disappeared by 6 h, (iii) very little dimer was present, (iv) significant fibril formation occurred at about 3.5 h and saturated at ~ 5.5 h, and (v) formation and growth of trimers was faster than 4- and 5-mers and all three saturated at ~ 5.5 h. The experiment starts off with the rapid breaking down of original insulin hexamers, which gives rise to a drastic increase of monomer concentration. During the second stage (1-4 h), a quasi steady-state of cluster distribution appears and the oligomer concentrations rise slowly at the expense of disappearing monomers [28]. After the wave front reaches a certain critical condition, sufficient fibril ends are formed to serve as active sites for further elongation. The autocatalytic nature of the newly formed fibrils ignites the creation of clusters rapidly through a positive feedback loop until the monomers are depleted and oligomers reach their steady state concentrations. These simulation results clearly describe the sigmoidal curves shown in Figure 3-2A. for the formation and disappearance of fibrils and proteins, respectively.

Since sigmoidal behavior for most amyloidogenic proteins has been observed, this similarity in the response of many proteins suggests a common mechanism [14, 15, 36]. We decided to test our model with fibril formation data from the literature for several other such proteins. First, Sup35 is a yeast translation termination factor known to assemble in a prion-like form with its N and M segments governing prion formation [17]. Likewise, A β -40 is a protein fragment that aggregates into amyloid plaques and has been found in the brains of Alzheimer's disease patients [5]. However, for proteins other than insulin we needed to replace the hexamer dissociation step with a fast misfolding reaction. Shown in **Fig. 3** are the fibrillation data for a NM amyloid fragment of Sup35 at 2.5 μ M

and the A β -40 segment at 80 μ M as well as the best fits (solid lines) [5, 17]. The coefficients of determination and kinetic rate parameters are listed in Table 3-2. The large R^2 values indicate the model fits the data well. For both NM and A β -40, the values

of the nucleation rates ($k_{nu,i}$) are several orders of magnitude faster than those for insulin. This result is consistent with reports in the literature that indicate the ease of forming fibrils with NM and A β -40 [5, 17]. This demonstrates the flexibility of the model and suggests that the mechanism among amyloid proteins may be similar. More importantly, this model can potentially serve as the template for comparing and unifying data sets across different protein experiments carried out under various operational conditions such as changing initial concentrations, seeding and stirring. These effects are addressed next.

Table 3-2. Rate constants obtained by fitting the kinetic model to various experimental conditions (with \pm one standard deviation)

Factors	Figure #	Exp. notes & Ref.	$k_{nu,i}$ ($\text{h}^{-1}\text{mM}^{-1}$)	$k_{fb,i}$ ($\text{h}^{-1}\text{mM}^{-1}$)	k_{fb} (h^{-1})	R^2
Solution	Fig. 2A	Insulin, abs@600nm	$3.54 \pm 2.12 \times 10^{-2}$	$2.73 \pm 0.66 \times 10^6$	$1.93 \pm 1.87 \times 10^3$	0.94
		Insulin, conc.	$4.72 \pm 1.60 \times 10^{-2}$	$3.85 \pm 3.59 \times 10^6$	$1.30 \pm 0.66 \times 10^3$	0.98
		Insulin, combined	$3.74 \pm 1.13 \times 10^{-2}$	$2.75 \pm 0.48 \times 10^6$	$1.84 \pm 0.42 \times 10^3$	0.95
	Fig. 3	Prion [17]	$7.10 \pm 6.73 \times 10^2$	$1.51 \pm 1.22 \times 10^4$	$1.26 \pm 2.04 \times 10^{-1}$	0.99
		A β 1-40 [5]	$1.38 \pm 0.53 \times 10^0$	$1.37 \pm 0.89 \times 10^6$	$3.02 \pm 2.64 \times 10^2$	0.99
Initial conc	Fig. 4A	Insulin, all concs [30]	$3.20 \pm 0.42 \times 10^{-1}$	$4.50 \pm 0.50 \times 10^5$	$4.00 \pm 0.88 \times 10^1$	0.92
Seeding	Fig. 5	Insulin, 0 & 10% [12]	$7.90 \pm 1.40 \times 10^{-2}$	$1.52 \pm 4.17 \times 10^6$	$1.99 \pm 1.16 \times 10^1$	0.87
Stirring	Fig. 6	Insulin, 80 rpm [43]	$1.43 \pm 0.75 \times 10^{-1}$	$4.20 \pm 1.15 \times 10^6$	$7.14 \pm 2.47 \times 10^0$	0.99
		Insulin, 160 rpm [43]	$2.68 \pm 4.12 \times 10^{-1}$	$1.27 \pm 5.27 \times 10^7$	$5.19 \pm 3.60 \times 10^1$	0.99

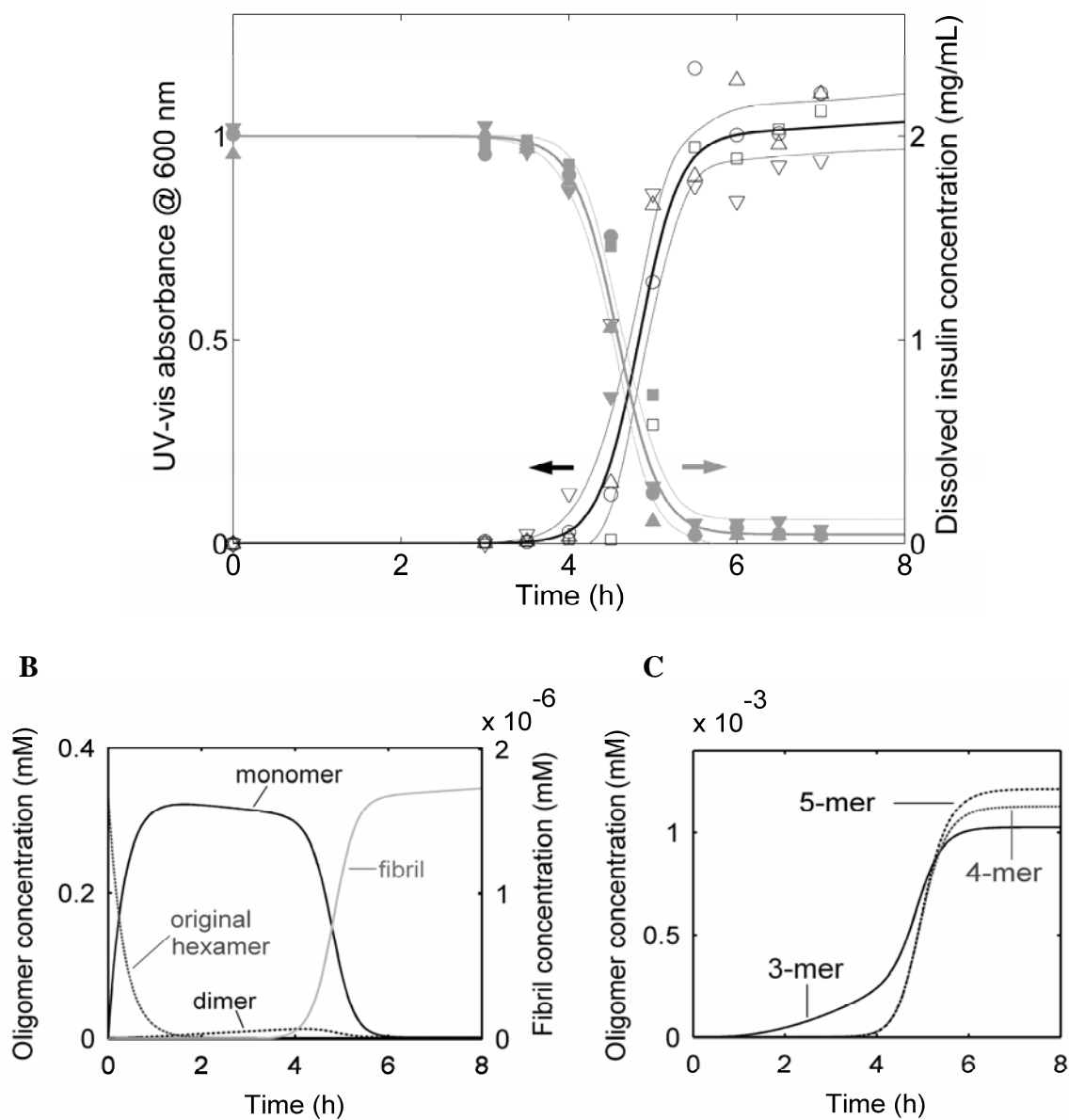


Figure 3-2 Insulin fibrillation in solution was monitored by UV-Vis spectroscopy. (A) The experimental data and simulated responses for two different assays: A600 (open symbols) for suspended fibrils and A280 (solid symbols) for total dissolved protein, respectively. Each symbol is for a single experimental run. The solid lines are the overall optimal nonlinear least square fit while the thin dotted lines represent the 95% confidence interval. (B) Simulated concentration profiles versus time for monomer, original hexamer, dimer, and fibril. (C) The corresponding profiles for 3-mer, 4-mer, and 5-mer.

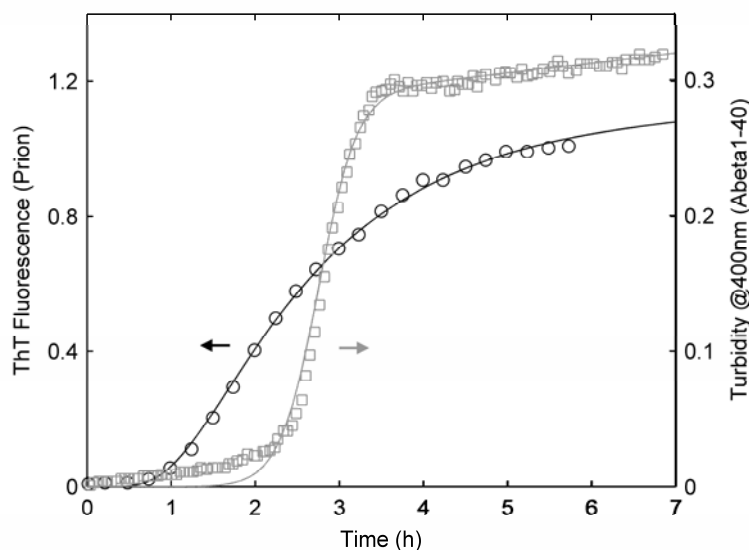


Figure 3-3 The fibrillation responses for a 2.5 μM NM amyloid fragment of Sup35 from yeast monitored by ThT fluorescence (open circles). Data source: Krishnan et al. [17]. The fibrillation responses for 80 μM A β 1-40 measured by turbidity assay (open squares). Data source: Evans et al. [5]. The solid lines are the optimal nonlinear least square fit.

3.3.2 *In vivo* fibrillation kinetics

Most of the *in vitro* fibrillation experiments only last for a few hours which is short compared to the disease progression of senile dementia. Modeling fibrillation *in vivo* is much more complex than that *in vitro* because of several practical reasons. First of all, there are potential interactions between fibrils and neurons. There are upstream reactions that lead to generation of amyloid monomers as well as down stream ones that decompose amyloid oligomers and fibrils. Also the transportation of biomolecules in living systems is hard to track and model. Second, the *in vivo* measurement itself is harder to perform as metabolism may interfere with chemical or immunoassaying. Therefore, the quality and quantity of the data are not as good as those *in vitro*. Finally, the physiological conditions *in vivo* are more difficult to control such as pH values, temperature, and ionic strength, etc.

Yet we adopted the same *in vitro* kinetic model of amyloid fibrillation for *in vivo* experimental data as a preliminary step toward full scale modeling. Cortical neurons of APP transgenic mice were observed by the multiphoton microscope which is a breakthrough technique for monitoring newly formed amyloid plaques. *In vivo* imaging of amyloid pathology was recorded after the addition of blue methoxy-XO4, the staining specific for amyloid deposition. As shown in Figure 3-4, the sizes of the plaques increased rapidly within the first day of experiment and stayed at about the same level afterwards. We used the same values of reaction rate constants yet changed the initial amyloid protein concentration. The initial concentration we used for this case was 0.7 mg/mL compared to the value 2 mg/mL we used for matching Figure 3-2. Granted that other physiological factors may affect the rate at

which amyloid proteins fibrillate, the time it took for significant amount of fibrils to form is roughly inversely proportional to the initial concentration of amyloid proteins. The following section discusses the concentration effects in details.

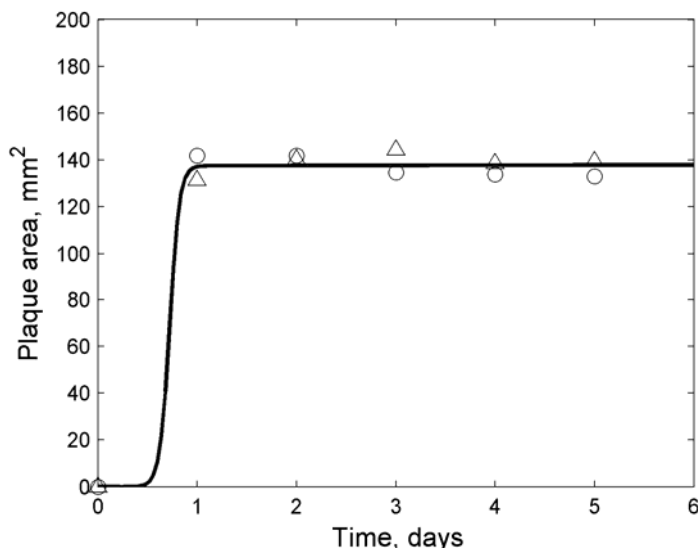


Figure 3-4 The *in vivo* fibrillation responses in cortical neurons of APP transgenic mice. Multiphoton Imaging techniques were used to track the size of amyloid beta plaque since its formation [26]. The experiment continued for about one week (open triangles and circles) with the simulation results by our model (solid line).

3.3.3 Initial concentration effects

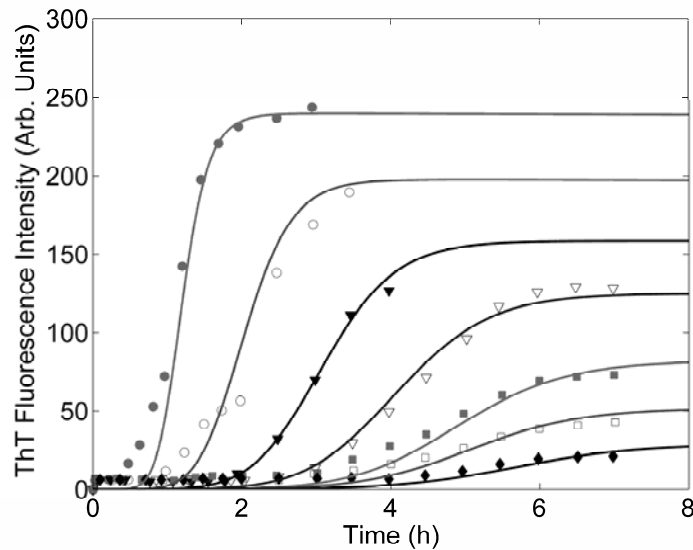
Data from Fink's group [30] showing the effect of varying initial concentration (0.2 to 20 mg/mL) of human recombinant insulin on the fibrillation are reproduced in Figure 3-5A. Clearly, the higher the initial concentration of insulin, the shorter the lag-time and the steeper the growth curve. However, as can be seen from the figure, the ThT intensity asymptotes for long times are not proportional to the initial amount of protein in the feed. This result coincides with other results in our group (unpublished). Thus, ThT fluorescence does not grow linearly with respect to the amount of fibers present. By applying a single set of kinetic rate constants for seven different initial concentrations, our initial simulations did show consistent trends. However, at first the simulated asymptote of each individual concentration could not match the experimental results.

In order to quantify the concentration results better, nonlinear effects from at least two possible sources should be considered; the non-ideal behavior of proteins at high concentrations and a possible artifact from the fluorescence ThT assay. The activity coefficients of proteins at high concentrations are typically not constants and should be considered in the model [1]. Second, as mentioned above, nonlinearity with the ThT signal exists perhaps because ThT measurements depends on the ThT:fibril formation which involves stoichiometric binding of both compounds [22]. This nonlinear relationship is unknown so the proportionality constants based on each curve was

estimated. The first step was to estimate the activity of insulin at each concentration based on the experimental data given a set of kinetic rate constants. Afterwards, the activity coefficients were computed by dividing the activity values by the original concentrations. Finally, the concentration of ThT:fibril complex was the product of proportional constant and asymptotic fibril concentration. The values of the activity coefficient and ThT:fibril complex concentration are summarized in Figure 3-5B. As expected from estimates using the equation of state, it can be seen from Figure 3-5B that the calculated activity coefficients decreased with an increase in the initial insulin concentration. On the other hand, since the amount of ThT added in each run was fixed regardless of the initial amount of insulin added, it became the limiting agent at high insulin concentration. Thus, ThT:fibril complex concentration did not rise linearly with increasing initial insulin concentration, but appeared to reach an asymptote.

After the adjustment regarding the nonlinearity, the simulated results by our model match the experimental data better. Yet additional experiments that measure the actual protein quantities by osmotic pressure, for example, and determine the multivariate relationship between ThT concentration, amyloid fibrils, and fluorescence signal would be useful in testing our hypothesis.

A



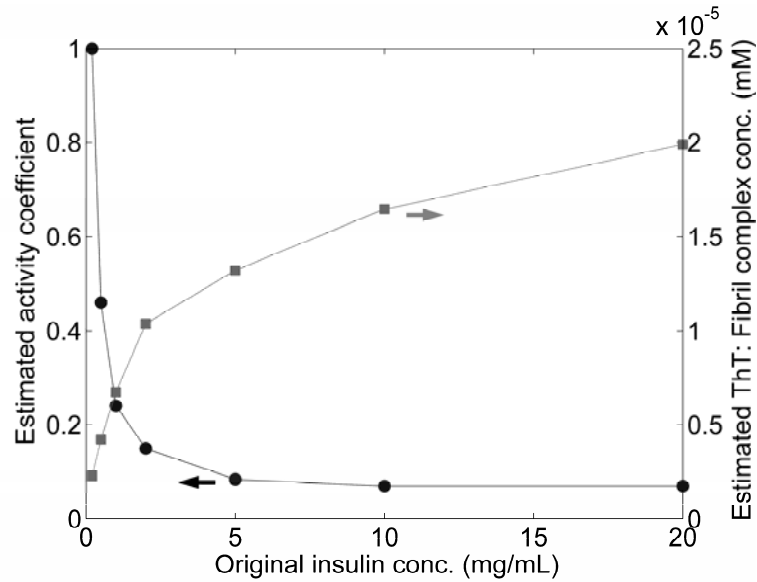
B

Figure 3-5 Initial concentration effects on insulin fibrillation were monitored by ThT fluorescence. (A) The experimental measurements and simulations of fibrillation responses starting at seven initial insulin concentrations: 20 mg/ml (solid circles), 10 mg/ml (open circles), 5.0 mg/ml (solid triangles), 2.0 mg/ml (open triangles), 1.0 mg/ml (solid squares), 0.5 mg/ml (open squares), and 0.2 mg/ml (solid diamonds). The solid lines are the optimal nonlinear least square fit. Data source: Nielsen, 2001 [30]. (B) The estimated activity coefficients (solid circles) and equilibrated ThT:fibril complex concentrations (solid squares) as functions of initial insulin concentrations. The lines are used to connect the calculated points and do not represent a fit.

3.3.4 Effects of seeding

The addition of fibril seeds to a solution that is in the process of forming fibrils shortens the lag time. This effect has been termed a “nucleation-dependent” phenomenon by Wood et al. [46]. They explained that the added seeds act as catalytic sites that induce conformational changes in the protein (α -synuclein) and accelerate the reaction rates; also Scheibel et al. [36] have termed this “nucleated conformational conversion”. In Figure 3-6 both the effect of adding seeds to the initial insulin solution (2 mg/ml) and our simulation results are shown [12]. For the simulations, a single set of rate constant values was used for both curves because seeding only increases the likelihood of collision but not the probability of the corresponding reaction actually taking place. Since only the weight of the added fibril seeds was reported, the number of reactive ends was not known (nor details about the length distribution of fibrils). Thus, the estimated initial fibril concentration was obtained by minimizing the total sum of squared errors from both data sets with and without seeding. The best estimate for the initial concentration of fibril was 2.53×10^{-7} mM for a 10 wt% addition of seeds. This low value supports the hypothesis that fibril ends were the reactive sites although fibrils were composed of a large number of monomers [40]. As can be seen from the fit of the model to the data in Figure 3-6, the model does not capture the effect of the shortened lag-time very accurately. A possible

reason was that there exists size distribution of the added seeds and clusters. Unfortunately, without knowledge of this distribution, an estimate of the total added number of fibril ends was made. This likely oversimplified the seeding processes.

The explanation of the seeding effect from this analysis is based on the fact that the rate constants for fibril growth were orders of magnitude larger than those for the nucleation process. Hence fibril growth could not take place unless sufficient amounts of nuclei were present. Therefore, the addition of seeded fibrils allows the system to by-pass the slow nucleation phase and reach the growth phase much faster and earlier.

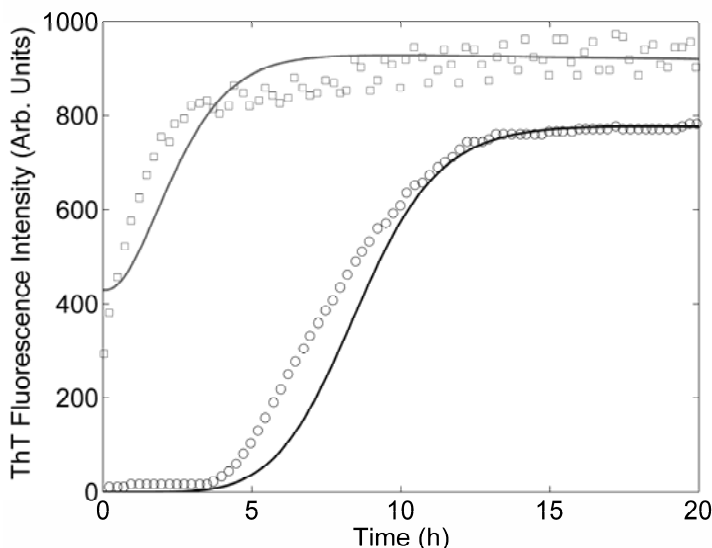


Figure 3-6 The measured and simulated fibrillation responses without seeding (open circles) and with 10 wt% seeding (open squares) were monitored by ThT fluorescence. The solid lines are the simulated responses with initial insulin concentration equal to 2 mg/ml. Data source: Hong and Fink [12].

3.3.5 Stirring effects

It has been reported that stirring or shaking can shorten the lag phase and speed up fibrillation process. One proposed reason for these effects was that agitation would increase the air-water interface and the presence of additional hydrophobic interfaces (air) would accelerate nucleation [43]. Other possible explanations include that additional mixing accelerates polymerization by breaking up large complexes and increasing the collision of reactive complexes with each other and with fiber ends [40]. Figure 3-7 contains the transient responses of measured as well as simulated dissolved insulin concentrations under different rotational speeds for an initial concentration of 0.6 mg/ml [43]. Both demonstrate that higher rotational speed results into faster fibrillation and shorter lag times. From Table 3-2, the rate constants increase for nucleation and for fibril formation with increased mixing. That is, the values of $k_{nu,1}$ and $k_{fb,1}$ roughly doubled and tripled, which suggest an increase in the mass transfer coefficients caused by a higher collision rate between monomers and oligomers as well as between monomers and fibrils.

The nearly four fold increase in k_{fb} indicates that the fibers were losing oligomers from the end of the fibrils to create new nuclei.

A simple film theory can be adopted to predict the apparent rate constants under the influence of both transport and reaction [20]. According to this theory, transport and reaction resistances are in parallel and additive. Hence, being limited by diffusion at first, the rate of stationary process may increase and become reaction-controlled under stirring. The faster rotation initially results in larger apparent rate constants but the process may eventually become reaction controlled. Beyond that point, even more vigorous stirring and hence convection would not speed up the reaction any longer. Measuring fibrillation responses under different rotational speed can help estimating the amount of kinetic energy needed to overcome the diffusion barrier.

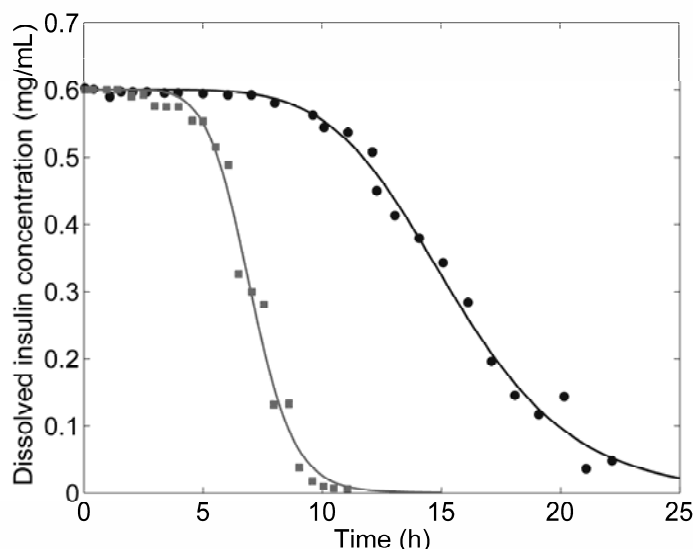


Figure 3-7 The dissolved insulin concentrations measured by UV absorbance starting from 0.6 mg/mL under different speeds of stirring: 80 revolutions per minute (rpm) (solid circles), and 160 rpm (solid squares). The solid lines are the optimal nonlinear least square fit. Data source: Slusky, 1991 [43].

3.4 Conclusion and further development

A three-stage model of fibrillation developed here was able to simulate the experimental data measured by us and by others. Hence, it provides a physical rationale for the generic sigmoidal (formation of fibrils) and inverse sigmoidal (loss of protein) fibrillation responses. In addition to the autocatalytic nature of fibril growth, the large difference between nucleation and growth rate constants lead to ultra-fast growth of fibrils after the lag period. Estimated from the ratio of the forward and backward nucleation rate constants, the Gibbs free energy change (ΔG°) of spontaneous reaction involving insulin monomers converted into nuclei was as large as 42.6 kJ/mol. In comparison with the logistic equation used by Nielsen et al. [30] and others, the computational model presented here can be simplified into the same functional form to fit

fibrillation responses. The physically meaningful rate constants in our model correspond to experimentally observable variables. Previous mechanistic models have provided insight, such as the enzymatic nature of the fibril ends [36], the critical size of nucleus [41], and detailed equations from population balances [33]. Yet most of these models do not explicitly predict the delay time and nor do they follow the sigmoidal behavior observed during experiments. For incorporating sets of nucleation and elongation reactions, the present model and the one proposed by Flyvbjerg et al. [6] both demonstrate better goodness-of-fit. Yet of these two models the detailed reactions schemes and predicted asymptotic oligomer concentration are different. It will take further work to differentiate these two models to determine the applicability of each one.

Based upon the profiles of insulin fibrillation, the values of the same rate constant ($k_{nu,1}$, $k_{fb,1}$ or k_{fb-}) estimated under different conditions of initial insulin concentration, seeding, or mixing effects were relatively close. On the contrary, prion and A β 1-40 demonstrate nucleation rates several orders faster than those for insulin, because both proteins are known to form fibrils under mild conditions (physiological pH and room or physiological temperature). For the initial insulin concentration effects, the simulated responses starting at different initial concentrations show a consistent trend with the experiments. The seeding effects of shorter lag time and faster growth rate were reflected in the predicted results by introducing a hypothetical amount of additional initial fibrils. The stirring raised the nucleation and elongation rates, which could be due to higher collision rates and more rapid dissociation of oligomers possibly from the ends of fibrils. Consequently higher reaction rates result in the shorter lag time and the steeper concentration profile.

Based on the work reported here, the following experiments are suggested to help further confirm a physical basis of the model and possibly indicate the molecular conformational properties that would be needed for inhibitors to bind to the nucleus or other oligomers so as to reduce their toxic affects. First, it is critically important to quantify the relationship between the output variables with the state variables of interest; i.e., match the spectroscopic measurements with the actual concentrations of fibrils. Second, one needs to track the temporal evolution of the oligomers (dimers, trimers... nucleus) and fibrils (i.e. fibril lengths and their temporal distribution) possibly by AFM to verify the critical nucleus size. Larger-size clusters could be followed using dynamic light scattering and isolated using a fractionation procedure together with a toxicity assay to determine actual pathogenic species [3, 24, 25, 35]. Third and fourth, with respect to seeding and agitation effects, a series of carefully designed experiments are needed [40]. For example, the number and size distribution of seeded fibrils should be known and varied prior to seeding so as to confirm the importance of the amino acids at the end of the fibrils or the total number of amino acids within the fibrils as reactive sites. In all the mixing or agitation experiments reported to date in the literature, the fundamental fluid mechanical properties (shear rate and distribution, vorticity, etc.) of the mixing conditions have not been reported. Clearly, what is needed is a well-controlled mixing experiment in which the sigmoidal fibrillation run is conducted under different and well-designed fluid mechanical conditions. Fifth, it could be very important to vary the temperature, pH and ionic strength during fibrillation. One could then estimate the activation energy and

activity coefficients for formation of oligomers and fibrils. Sixth, based on molecular structures of several amyloid peptides that have been previously simulated [27, 29], the aggregation rate constants among oligomers could be estimated. In brief, our model extracts rate constants from transient experiments and bridges the gap between experiments and molecular simulation. This methodology can be used to evaluate the potential of fibrillation inhibitors or enhancers by the decrease or increase in reaction rates they introduce [23].

In summary, amyloid proteins undergo three stages: misfolding, nucleation, and elongation, before turning into fibril aggregates. Validated by many experimental results, this mechanistic model is applicable for various types of proteins, and for fibrillation under different environmental conditions. Further experiments tracking oligomer concentrations and theoretical analysis of molecular simulations are promising for determining pathological species and the desired properties of fibrillation inhibitors.

Table 3-3. The summary of nomenclature

Symbols	Units	Definitions
A_0	mM	Initial insulin concentration
A_1	mM	Insulin monomer or insulin monomer concentration
A_{hex}	mM	Original insulin hexamer or its concentration
A_i	mM	Insulin cluster consisting of i monomers or its concentration
b	mM^{-1}	Proportional constant relating fibril concentration to exp signal
d_{AF}	m	The mean free path between monomer and fibril
D_{A_i}	m^2s^{-1}	Diffusivity of oligomer A_i
D_F	m^2s^{-1}	Diffusivity of fibril
ΔG°	kcal/mol	Gibbs free energy of the reaction of monomers becoming $(n-1)$ -mers
f	-	Our fibrillation model expressed as a function
F	mM	Fibrils or fibril concentration
i	#	Index of nucleation or elongation reaction or the size of cluster
J_{hex}	$\text{mM}\cdot\text{h}^{-1}$	The reaction flux of original insulin decomposition
$J_{nu,i}$	$\text{mM}\cdot\text{h}^{-1}$	The flux of i -th nucleation reaction
$J_{fb,i}$	$\text{mM}\cdot\text{h}^{-1}$	The flux of i -th fibrillation reaction
k_{app}	h^{-1}	The apparent growth rate of fibril, which is equal to $1/\tau$
K_c	$\text{mM}^{-(n-2)}$	Equilibrium constant between monomers and $(n-1)$ -mers
k_{hex}	h^{-1}	Reaction rate constant of original insulin decomposition
k_{fb-}	h^{-1}	General reverse rate constant of fibrillation reaction
$k_{fb,1}$	$\text{h}^{-1}\text{mM}^{-1}$	Forward rate constant of the first fibrillation reaction
$k_{fb,i}$	$\text{h}^{-1}\text{mM}^{-1}$	Forward rate constant of i -th fibrillation reaction
$k_{fb,-i}$	h^{-1}	Reverse rate constant of i -th fibrillation reaction
$k_{nu,1}$	$\text{h}^{-1}\text{mM}^{-1}$	Forward rate constant of the first nucleation reaction
k_{nu-}	h^{-1}	General reverse rate constant of nucleation reaction
$k_{nu,i}$	$\text{h}^{-1}\text{mM}^{-1}$	Forward rate constant of i -th nucleation reaction
$k_{nu,-i}$	h^{-1}	Reverse rate constant of i -th nucleation reaction
m_i, m_f	h^{-1}	The slope of initial and final fibrillation response curve, respectively
n	#	Critical number of monomers in a nucleus
n_{exp}	#	The number of experimental data points
N	#	The average size of fibrils in terms of number of monomer
\tilde{N}	mol^{-1}	Avogadro constant
$\Phi(\underline{\theta})$	-	The objective function to be optimized with respect to $\underline{\theta}$
R	J/molK	Ideal gas constant, 8.314
R^2	-	Coefficient of determination
R_{A_i}	m	Characteristic length of oligomer A_i
r_1, r_2	mM	The first and second roots of the fibril quadratic equation
t_0	h	The time to 50% of maximal signal or the time of inflection point
t_i	h	The time of i -th experimental data point
$t_{v,\alpha/2}$	-	Student's t-distribution with degree of freedom v , significance level α
τ	h	The time constant of fibril growth and it is equal to $1/k_{app}$
$\underline{\theta}$	-	The vector of parameters to be estimated

1. Avena SM, Bogle IDL, Pessoa FLP (1997) An activity coefficient model for proteins. *Biotechnol Bioeng* 55:65-71
2. Bird RB, Stewart WE, Lightfoot EN (2002) *Transport Phenomena*. John Wiley and Sons, New York City, NY
3. Bitan G, Lomakin A, Teplow DB (2001) Amyloid β -protein oligomerization pre-nucleation interactions revealed by photo-induced cross-linking of unmodified proteins. *J Biol Chem* 276:35176-35184
4. Collins SR, Douglass A, Vale RD, Weissman JS (2004) Mechanism of prion propagation: amyloid growth occurs by monomer addition. *PLoS Biol* 2:1582–1590
5. Evans KC, Berger EP, Cho CG, Weisgraber KH, Lansbury Jr PT (1995) Apolipoprotein E is a kinetic but not a thermodynamic inhibitor of amyloid formation: implications for the pathogenesis and treatment of Alzheimer disease. *Proc Natl Acad Sci USA* 92:763-767
6. Flyvbjerg H, Jobs E, Leibler S (1996) Kinetics of self-assembling microtubules: an "inverse problem" in biochemistry. *Proc Natl Acad Sci USA* 93:5975-5979
7. Fogler HS (1998) *Elements of chemical reaction engineering*. Prentice-Hall, Upper Saddle River, NJ.
8. Gill R (1994) Protein engineering of insulin-like growth factor. PhD Thesis. In: University of London, London, UK
9. Gosal WS, Morten IJ, Hewitt EW, Smith DA, Thomson NH, Radford SE (2005) Competing pathways determine fibril morphology in the self-assembly of β 2-microglobulin into amyloid. *J Mol Biol* 351:850-864
10. Hasegawa K, Ono K, Yamada M, Naiki H (2002) Kinetic modeling and determination of reaction constants of Alzheimer's β -amyloid fibril extension and dissociation using surface plasmon resonance. *Biochemistry* 41:13489–13498
11. Hassiepen U, Federwisch M, Mulders T, Wollmer A (1999) The lifetime of insulin hexamers. *Biophys J* 77:1638-1654
12. Hong DP, Fink AL (2005) Independent heterologous fibrillation of insulin and its β -chain peptide. *Biochemistry* 44:16701-16709
13. Jimenez JL, Nettleton EJ, Bouchard M, Robinson CV, Dobson CM, Saibil HR (2002) The protofilament structure of insulin amyloid fibrils. *Proc Natl Acad Sci USA* 99:9196–9201
14. Kaye R, Head E, Thompson JL, McIntire TM, Milton SC, Cotman CW, Glabe CG (2003) Common structure of soluble amyloid oligomers implies common mechanism of pathogenesis. *Science* 300:486-489
15. Khurana R, Ionescu-Zanetti C, Pope M, Li J, Nielson L, Ramirez-Alvarado M, Regan L, Fink AL, Carter SA (2003) A general model for amyloid fibril assembly based on morphological studies using atomic force microscopy. *Biophys J* 85:1135-1144
16. Kingsland SE (1995) *Modeling Nature*. University of Chicago Press, Chicago, IL
17. Krishnan R, Lindquist SL (2005) Structural insights into a yeast prion illuminate nucleation and strain diversity. *Nature* 435:765-772

18. Lashuel HA, Lansbury PT (2006) Are amyloid diseases caused by protein aggregates that mimic bacterial pore-forming toxins? Cambridge University Press, Cambridge, UK.
19. Lee CC, Nayak A, Belfort G, McRae GJ (2006) A mathematical model of amyloid fibrillation: the case for insulin. In: Biophysical Society Conference. Salt Lake City, Utah.
20. Levenspiel O (1999) Chemical Reaction Engineering. John Wiley and Sons, New York City, NY
21. LeVine III H (2005) Multiple ligand binding sites on A β (1–40) fibrils. Protein Folding Symposium #7, Amyloids 12:5-14
22. LeVine III H (1999) Quantification of beta-sheet amyloid fibril structures with thioflavin T. Methods Enzymol 309:274-284
23. Liu Y, Lashuel HA, Choi S, Xing X, Case A, Ni J, Yeh LA, Cuny GD, Stein RL, Lansbury PT (2003) Discovery of inhibitors that elucidate the role of UCH-L1 activity in the H1299 lung cancer cell line. Chem Biol 10:837-846
24. Lomakin A, Teplow DB, Kirschner DA, Benedek GB (1997) Kinetic theory of fibrillogenesis of amyloid beta-protein. Proc Natl Acad Sci USA 94:7942–7947
25. Manno M, Craparo EF, Martorana V, Bulone D, San Biagio PL (2006) Kinetics of insulin aggregation: disentanglement of amyloid fibrillation from large-size cluster formation. Biophys J 90:4585-4591
26. Meyer-Luehmann M, Spires-Jones TL, Prada C, Garcia-Alloza M, de Calignon A, Rozkalne A, Koenigsnecht-Talboo J, Holtzman DM, Bacskai BJ, Hyman BT (2008) Rapid appearance and local toxicity of amyloid- β plaques in a mouse model of Alzheimer's disease. Nature 451:720-724
27. Nelson R, Sawaya MR, Balbirnie M, Madsen AO, Riekel C, Grothe R, Eisenberg D (2005) Structure of the cross- β spine of amyloid-like fibrils. Nature 435:773-778
28. Neu JC, Cañizo JA, Bonilla LL (2002) Three eras of micellization. Phys Rev E 66:61406
29. Nguyen HD, Hall CK (2004) Molecular dynamics simulations of spontaneous fibril formation by random-coil peptides. Proc Natl Acad Sci USA 101:16180-16185
30. Nielsen L, Khurana R, Coats A, Frokjaer S, Brange J, Vyas S, Uversky VN, Fink AL (2001) Effect of environmental factors on the kinetics of insulin fibril formation: elucidation of the molecular mechanism. Biochemistry 40:6036-6046
31. Osterbye T, Jorgensen KH, Fredman P, Trantum-Jensen J, Kaas A, Brange J, Whittingham JL, Buschard K (2001) Sulfatide promotes the folding of proinsulin, preserves insulin crystals, and mediates its monomerization. Glycobiology 11:473-479
32. Padrick SB, Miranker AD (2002) Islet amyloid: phase partitioning and secondary nucleation are central to the mechanism of fibrillogenesis. Biochemistry 41:4694-4703
33. Pallitto MM, Murphy RM (2001) A mathematical model of the kinetics of β -amyloid fibril growth from the denatured state. Biophys J 81:1805-1822

34. Pasternack RF, Gibbs EJ, Sibley S, Woodard L, Hutchinson P, Genereux J, Kristian K (2006) Formation kinetics of insulin-based amyloid gels and the effect of added metalloporphyrins. *Biophys J* 90:1033-1042
35. Quist A, Doudevski I, Lin H, Azimova R, Ng D, Frangione B, Kagan B, Ghiso J, Lal R (2005) Amyloid ion channels: a common structural link for protein-misfolding disease. *Proc Natl Acad Sci USA* 102:10427-10432
36. Scheibel T, Bloom J, Lindquist SL (2004) The elongation of yeast prion fibers involves separable steps of association and conversion. *Proc Natl Acad Sci USA* 101:2287-2292
37. Seber GAF, Wild CJ (2003) *Nonlinear Regression*. John Wiley and Sons, New York City, NY
38. Seinfeld JH, Pandis SN (1998) *Atmospheric chemistry and physics: from air pollution to climate change*. John Wiley and Sons, New York City, NY
39. Selkoe DJ (2004) Cell biology of protein misfolding: The examples of Alzheimer's and Parkinson's diseases. *Nat Cell Biol* 6:1054-1061
40. Serio TR, Cashikar AG, Kowal AS, Sawicki GJ, Moslehi JJ, Serpell L, Arnsdorf MF, Lindquist SL (2000) Nucleated conformational conversion and the replication of conformational information by a prion determinant. *Science* 289:1317-1321
41. Shoghi-Jadid K, Barrio JR, Kepe V, Wu HM, Small GW, Phelps ME, Huang SC (2005) Imaging β -amyloid fibrils in Alzheimer's disease: a critical analysis through simulation of amyloid fibril polymerization. *Nucl Med Biol* 32:337-351
42. Sipe JD (2005) *Amyloid Protein: The Beta Sheet Conformation and Disease*. John Wiley and Sons, New York City, NY
43. Sluzky V, Tamada JA, Klibanov AM, Langer R (1991) Kinetics of insulin aggregation in aqueous solutions upon agitation in the presence of hydrophobic surfaces. *Proc Natl Acad Sci USA* 88:9377-9381
44. Uversky VN, Li J, Fink AL (2001) Metal-triggered structural transformations, aggregation, and fibrillation of human α -synuclein. A possible molecular link between Parkinson's disease and heavy metal exposure. *J Biol Chem* 276:44284-44296
45. Wang F, Hull RL, Vidal J, Cnop M, Kahn SE (2001) Islet amyloid develops diffusely throughout the pancreas before becoming severe and replacing endocrine cells. *Diabetes* 50:2514-2520
46. Wood SJ, Wypych J, Steavenson S, Louis JC, Citron M, Biere AL (1999) α -synuclein fibrillogenesis is nucleation-dependent *J Biol Chem* 274:19509-19512